*Proc. Natl. Acad. Sci. USA*
Vol. 96, pp. 8229–8234, July 1999
Neurobiology

# Structure of tau exon 10 splicing regulatory element RNA and destabilization by mutations of frontotemporal dementia and parkinsonism linked to chromosome 17

**(alternative mRNA splicing/intronic mutations/stem-loop RNA structure)**

LUCA VARANI*, MASATO HASEGAWA*, MARIA GRAZIA SPILLANTINI†, MICHAEL J. SMITH*, JILL R. MURRELL‡, BERNARDINO GHETTI‡, AARON KLUG*, MICHEL GOEDERT*, AND GABRIELE VARANI*§

*Medical Research Council Laboratory of Molecular Biology, Hills Road, Cambridge CB2 2QH, United Kingdom; †Department of Neurology, E. D. Adrian Building, University of Cambridge, Robinson Way, Cambridge CB2 2PY, United Kingdom; and ‡Department of Pathology and Laboratory Medicine, Indiana University School of Medicine, Indianapolis, IN 47202

*Contributed by Aaron Klug, May 6, 1999*

**ABSTRACT** **Coding region and intronic mutations in the tau gene cause frontotemporal dementia and parkinsonism linked to chromosome 17. Intronic mutations and some missense mutations increase splicing in of exon 10, leading to an increased ratio of four-repeat to three-repeat tau isoforms. Secondary structure predictions have led to the proposal that intronic mutations and one missense mutation destabilize a putative RNA stem-loop structure located close to the splice-donor site of the intron after exon 10. We have determined the three-dimensional structure of this tau exon 10 splicing regulatory element RNA by NMR spectroscopy. We show that it forms a stable, folded stem-loop structure whose thermodynamic stability is reduced by frontotemporal dementia and parkinsonism linked to chromosome 17 mutations and increased by compensatory mutations. By exon trapping, the reduction in thermodynamic stability is correlated with increased splicing in of exon 10.**

Abundant neurofibrillary lesions made of the microtubule-associated protein tau constitute a defining neuropathological characteristic of Alzheimer's disease (1). Filamentous tau protein deposits are also the defining characteristic of other neurodegenerative diseases, many of which are frontotemporal dementias or movement disorders that have been subsumed under the heading of "Pick complex" (1, 2). Recent work has shown that mutations in the tau gene cause frontotemporal dementia and parkinsonism linked to chromosome 17 (FTDP-17) (3–13). Known mutations are either coding region or intronic mutations located close to the splice-donor site of the intron after exon 10 of the tau gene. Many coding region mutations produce a reduced ability of tau to interact with microtubules, thus probably setting in motion the mechanisms that lead to the formation of tau filaments (13–16). Four mutations have been described at positions +3, +13, +14, and +16 of the intron after exon 10 (with the first nucleotide of the splice-donor site taken as +1) (4, 5, 10, 11). The S305N mutation in exon 10 also is located close to this splice-donor site (9).

Six tau isoforms are produced in adult human brain by alternative mRNA splicing from a single gene (17–19). They differ from each other by the presence or absence of 29-aa or 58-aa inserts located in the amino-terminal half and a 31-aa repeat located in the carboxyl-terminal half. Inclusion of the latter, which is encoded by exon 10 of the tau gene, gives rise to the three tau isoforms with four repeats each (17, 18); the other three isoforms have three repeats each (18). The repeats and some adjoining sequences constitute the microtubule-binding domains of tau (20, 21). Similar levels of three-repeat and four-repeat tau isoforms are found in normal cerebral cortex (22), and the tau filaments from Alzheimer's disease brain contain all six tau isoforms in a hyperphosphorylated state (23).

Three of the intronic mutations (at positions +13, +14, and +16) and the S305N mutation at position −1 have been shown to increase splicing in of exon 10 (4, 24). Increased production of tau isoforms with four repeats has been described in brain tissue from individuals with three of the intronic mutations (5, 11, 15). The overproduction of four-repeat tau thus is sufficient to lead to a dementing disease (25). A potential mechanism underlying the overproduction of four-repeat tau isoforms was proposed, based on the prediction that a putative RNA stem-loop structure at the boundary between exon 10 and the intron after exon 10 would be destabilized by the intronic mutations (4, 5). We have investigated this proposal by determining the three-dimensional structure of the tau exon 10 splicing regulatory element RNA by using NMR spectroscopy. We show here that it does indeed form a stable, folded stem-loop structure that differs, however, in several respects from previous predictions. We also show that the intronic FTDP-17 mutations destabilize the stem-loop structure and that this destabilization is correlated with increased splicing in of exon 10.

## METHODS

**RNA Sample Preparation.** RNA oligonucleotides extending from nucleotides −5 to +19 were prepared by *in vitro* transcription using T7 RNA polymerase and synthetic DNA templates. RNA was purified by PAGE, followed by electroelution, extensive dialysis, and size exclusion chromatography (26). Isotopically labeled samples (100% $^{13}C$-$^{15}N$) were prepared in the same manner, by using suitably isotopically labeled nucleoside triphosphate precursors. They were prepared from isotopically labeled NMPs (CIL, Cambridge, MA) after rephosphorylation and purification by filtration through 0.2-$\mu$m filters, followed by several cycles of ethanol precipitation. Samples for UV melting experiments were dialyzed against 150 mM NaCl, 0.1 mM EDTA in 10 mM sodium phosphate buffer, pH 6.7. Samples for NMR were dialyzed against low-salt buffer consisting of 10 mM sodium phosphate buffer, pH 6.7, so as to reduce the likelihood of RNA dimer-

The publication costs of this article were defrayed in part by page charge payment. This article must therefore be hereby marked "*advertisement*" in accordance with 18 U.S.C. §1734 solely to indicate this fact.

PNAS is available online at www.pnas.org.

Abbreviations: FTDP-17, frontotemporal dementia and parkinsonism linked to chromosome 17; NOE, nuclear Overhauser effect.

Data deposition: The atomic coordinates have been deposited in the Protein Data Bank, www.rcsb.org (PDB ID code 1Qc8).

§To whom reprint requests should be addressed. e-mail: gv1@mrc-lmb.cam.ac.uk.

ization. At the high concentrations required for biophysical studies, RNA has the potential to form dimeric structures. The presence of the stem-loop structure was unambiguously established from the very favorable linewidth and relaxation properties of the NMR resonances and from diffusion measurements that directly monitor the molecular mass of the sample (27). The RNA concentrations for the UV melting experiments were 1–2 $\mu$M. They were 0.8–1.5 mM for the NMR experiments.

**UV Melting.** UV melting experiments were recorded on a CARY UV/VIS spectrophotometer (Varian) equipped with a temperature-controlled heating unit. The heating rate was 1°C/min, and the data could be reproduced within experimental error after one heating/cooling cycle. Reproducibility of the melting temperatures was better than 2°C in independent experiments. We observed two separate transitions in all melting experiments, one occurring at low temperature and a second occurring at a higher temperature. The higher temperature transition corresponds to the melting of the secondary structure as observed by NMR. The lower transition is likely to correspond to the melting of duplex species that are favored in the conditions of the UV melting experiments (150 mM NaCl).

**NMR Spectroscopy.** NMR spectra were recorded on Bruker AMX-500 or DMX-600 spectrometers operating at 500 Mhz and 600 Mhz, respectively, and equipped with triple resonance, actively shielded gradient coils. All data were obtained at 27°C, with the exception of some $^{1}H$-$^{15}N$ correlated spectra and nuclear Overhauser effect (NOE) spectroscopy data that were repeated under conditions of low temperature (5–10°C) and pH (5.0–5.5), to allow identification of marginally stable hydrogen-bonded base pairs from the lower stem and the last A-U base pair at the stem-loop junction. Spectral assignments were obtained by standard methods (28). Experimental constraints for structure determination consisted of hydrogen bonding, scalar coupling, and NOE-based distance constraints. Hydrogen bonding constraints were obtained from the identification of slowly exchanging imino resonances and intra-base pair NOEs typical of Watson-Crick base pairs. They were supplemented with very weak planarity restraints to obtain planar hydrogen bonds. Dihedral angle constraints were obtained from the analysis of two- and three-dimensional correlated experiments, as described (28). NOE-based distance constraints were obtained from the analysis of two- and three-dimensional experiments recorded at different mixing times. Protons whose distance is fixed or constrained within narrow limits by the covalent geometry were used to calibrate the distance constraints. The statistics for the experimental constraints are shown in Table 1. Structures were calculated from completely random starting coordinates by using an X-PLOR-based simulated annealing protocol (28). Of 50 starting structures, 33 converged structures were selected based on agreement with the experimental data and their good covalent geometry. Nonconverged structures were identified from a clear increase in the pseudoenergy term corresponding to violations of experimental constraints. Structural statistics are summarized in Table 1.

**Exon Trapping.** The wild-type construct and constructs with the +3, +13, +14, and +16 intronic mutations were used. The tau sequences contained exon 10, as well as 34 nt of upstream intronic sequence and 85 nt of downstream intronic sequence. PCR products were subcloned into the splicing vector pSPL3, and exon trapping was done as described (24). PCR products were verified by DNA sequencing.

**Extraction of Soluble tau.** Frontal cortex from three patients with the +3 intronic mutation and three age-matched controls was used. Soluble tau was extracted and dephosphorylated, as described (5). Tau proteins were analyzed by 10% SDS/PAGE and blotted onto Immobilon N (Millipore). Blots were incubated overnight at 4°C with anti-tau antibodies BR133 and BR134 (diluted 1:1,000), which recognize the amino and carboxyl termini of tau, respectively (18). Tau bands were visualized by using the avidin-biotin Vectastain system (Vector Laboratories) and 3,3-diaminobenzidine as the substrate. The intensities of the tau bands were quantified by using the National Institutes of Health IMAGE program and expressed as the ratios of four-repeat to three-repeat tau isoforms.

Table 1. Experimental constraints and structure statistics

| | |
|---|---|
| Experimental constraints | |
| NOE distance constraints | 564 |
| Intraresidue | 331 |
| Sequential | 181 |
| Long and medium range | 52 |
| Hydrogen bonding and planarity constraints | 90 |
| Dihedral constraints | 124 |
| Total experimental constraints | 778 |
| (Average number per nucleotide) | 31.1 |
| Structure analysis* | |
| Average NOE violations in converged structure (>0.2 Å) | 0 |
| Angle violations in converged structures (>5°) | 0 |
| rms deviation from average structure (Å)† | |
| Full structure | 3.18 Å ± 0.56 |
| Double-helical stem (G−1–A5; U12–C17) | 0.93 Å ± 0.27 |
| Bulge loop (C−2–A5; U12–G18) | 2.60 Å ± 0.48 |
| Loop (A5-U12) | 2.93 Å ± 0.45 |

*Average deviations from ideal covalent geometry are comparable to those in other publications from our laboratory (28).
†Calculated more than 33 converged structures of 50 calculated structures.

## RESULTS

**Secondary Structure and Thermodynamic Stability of Wild-Type and Mutant Tau Exon 10 Splicing Regulatory Elements.** We synthesized oligonucleotides representing the wild-type regulatory element and the four sequence variants with mutations at positions +3, +13, +14, and +16 (Fig. 1) identified in familial FTDP-17 cases. We also synthesized an oligonucleotide containing the S305N mutation at position −1 and two additional oligonucleotides containing compensatory mutations that restore Watson-Crick base pairing within the predicted stem loop. Although this possibility was not immediately appreciated (4), the region with potential secondary structure extends beyond nucleotides −1 and +16 and includes nucleotides −5 to +19 (5). Oligonucleotides covering this region were prepared and NMR spectroscopy used to verify that the predicted secondary structure was present. One-dimensional NMR spectra of wild-type sequence were recorded at 35°C and found to contain the signature expected for three Watson-Crick G-C base pairs and two A-U base pairs (Fig. 2). Spectra recorded at lower temperature and pH showed an additional G-C base pair, as well as an additional A-U base pair (not shown). Analysis of NOE spectroscopy spectra led to the straightforward assignment of individual resonances, thus demonstrating that the tau exon 10 splicing regulatory element RNA forms the predicted stem loop. Analogous data recorded for each of the four sequence variants showed the presence of related secondary structures (Fig. 2), which was proved by obtaining spectral assignments for the various mutant oligonucleotides. The only exception was the +3 variant, for which the NMR data could not be clearly interpreted; this observation is attributable either to conformational variability or to the formation of a structure significantly different from that drawn in Fig. 1.

Having established the formation of the predicted stem-loop structure, we next investigated whether the intronic mutations in tau reduce the stability of the structure. NMR spectra

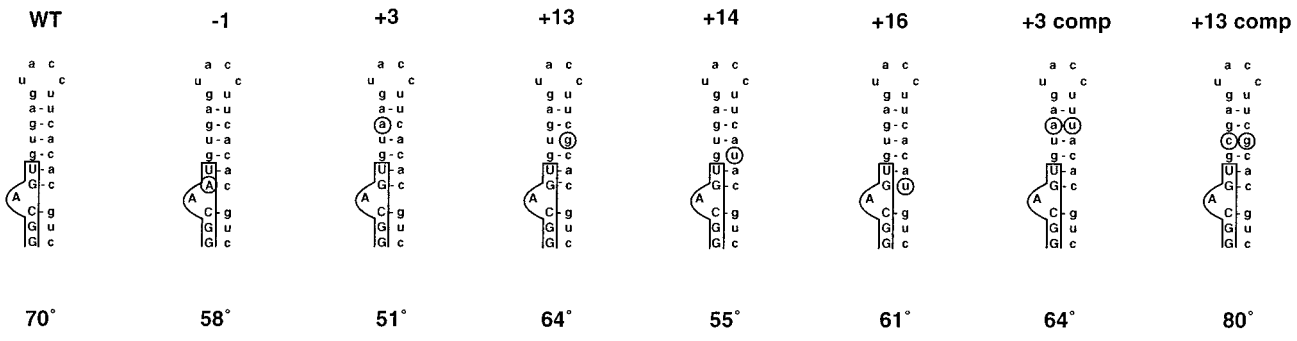


FIG. 1. Sequences and secondary structures of wild-type (WT) and mutant human tau exon 10 splicing regulatory elements. The sequences shown extend from nucleotides −5 to +19. Exonic sequences are boxed and shown in capital letters, and intronic sequences are shown in small letters, with the FTDP-17 mutations (at positions −1, +3, +13, +14 and +16) circled. For compensatory mutations (+3 comp and +13 comp), nucleotides that differ from the wild-type sequence are circled. Nucleotides involved in base pairs conclusively identified in this study are connected by a dash. The g nucleotide of the gu splice-donor site is designated +1, and the preceding U is designated zero. The bulged A is at position −2. Melting temperatures ($T_m$) are given below each sequence.

recorded at 45°C were strikingly different for the wild type and each of the mutant exon 10 splicing regulatory elements (Fig. 2). Signals corresponding to the base pairs depicted in Fig. 1 were clear in the wild-type sequence, but had disappeared at 45°C for each of the four intronic mutants. This behavior is observed when RNA secondary structure begins to unfold. Quantitative results were obtained by UV spectroscopy, because the unfolding of RNA secondary structure leads to an increase in UV absorption at 260 nm.

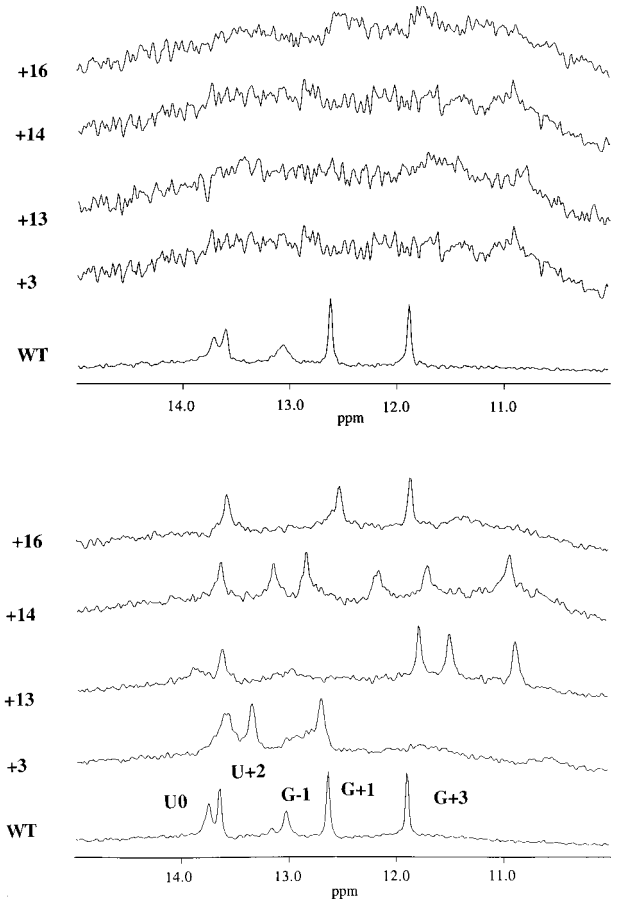


FIG. 2. NMR spectra of wild-type (WT) and mutant human tau exon 10 splicing regulatory elements. The spectra were recorded at 35°C (*Lower*) and 45°C (*Upper*). Only base NH resonances from Watson-Crick or G·U base pairs are observed in this region of the spectrum. Each stable G-C (G-1, G+1, G+3) or A-U (U0, U+2) base pair produces an observable NH signal, whereas each G·U base pair provides two observable NH resonances; the latter are observed between 10 and 12 ppm. From bottom to top, spectra correspond to that of the WT sequence, followed by those of the intronic +3, +13, +14, and +16 mutants, as indicated. Spectral assignments of the WT sequence indicate the nucleotides the exchangeable resonance belongs to.

We recorded a set of UV melting curves ($OD_{260}$ as a function of temperature) for the wild type and the seven mutant splicing regulatory elements (Fig. 1). The melting temperature, defined as the midpoint of the transition from fully structured to fully unstructured RNA, was estimated from the maximum in the derivative of the UV melting profile. The thermodynamic stability of the tau exon 10 splicing regulatory element was found to be exquisitely sensitive to sequence, with a drop of 19°C between the wild-type sequence and the +3 mutant, the least stable mutant. The reduction in temperature was 15°C for the +14 mutant, 12°C for the −1 mutant, 9°C for the +16 mutant, and 6°C for the +13 mutant (Fig. 1). The reduction in melting temperature for the regulatory element with the +3 compensatory mutation was only 6°C, and the regulatory element with the +13 compensatory mutation (C-G) was significantly more stable than the wild-type sequence (U-A) (Fig. 1).

Exon trapping analysis in transfected COS7 cells provided evidence for a quantitative correlation between thermodynamic stability of the RNA regulatory element and splice site utilization (Fig. 3). We compared a wild-type tau exon 10 construct with constructs carrying the +3, +13, +14, and +16 intronic mutations. As shown previously (4), the +13, +14, and +16 mutations increased the splicing in of exon 10, when compared with the wild-type construct. The +3 mutation also increased splicing in of exon 10. Based on three independent transfection experiments, the +3 mutation led to a 30-fold increase in the splicing in of exon 10, as compared with a 14-fold increase for the +14 mutation, a 7.5-fold increase for the +16 mutation, and a 7-fold increase for the +13 mutation (Fig. 3). We previously showed that the −1 mutation produces a 25-fold increase in the splicing in of exon 10 (24). We determined the ratios of soluble four-repeat to three-repeat tau isoforms in frontal cortex from patients with the +3 mutation. This ratio in controls (0.8 ± 0.08) was significantly lower than in patients with the +3 mutation (1.84 ± 0.24) ($P < 0.0001$, $n = 3$).

**Three-Dimensional Structure of Human tau Exon 10 Splicing Regulatory Element RNA.** The three-dimensional structure of the wild-type tau exon 10 splicing regulatory element was determined by heteronuclear multidimensional NMR using isotopically labeled RNA. Statistics of data collection and the final structure are shown in Table 1. A view of a converged structure highlighting the five sites where mutations occur is shown in Fig. 4.

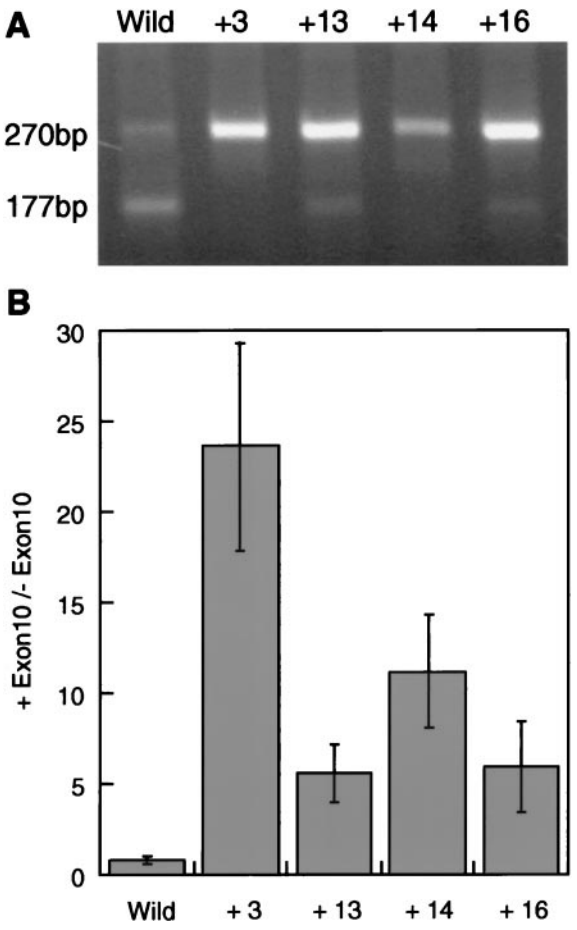


FIG. 3. Exon trapping analysis of the effects of the +3, +13, +14, and +16 intronic FTDP-17 mutations on the splicing of exon 10 of the tau gene. (*A*) Ethidium bromide-stained agarose gel of nested PCR products. The 270-bp band contains exon 10, whereas the 177-bp band lacks exon 10. A single experiment is shown. Similar results were obtained in three separate transfection experiments. (*B*) Quantitative analysis of exon trapping of wild-type construct and constructs with the +3, +13, +14, and +16 intronic mutations. The results are expressed as means ± SD ($n = 3$) of the ratios of exon 10-containing (+Exon 10) over exon 10-lacking (−Exon 10) transcripts.

The upper part of the tau exon 10 splicing regulatory element RNA forms a stable stem loop with a regular RNA A-form double helix of 6 bp, which is capped by a flexible apical loop of 6 nt. The apical loop does not form a stable structure, but rather adopts multiple conformations that are in rapid exchange on a time scale faster than 1 ms. The G·U base pair predicted to cap the double-helical stem does not form. The conformation of the double-helical 6-bp stem is typical of the A-form family of RNA structures. FTDP-17 mutations disrupt this regular structure by introducing non-Watson-Crick base pairs or mismatches that distort the RNA double helix and reduce its thermodynamic stability. The lower part of the structure is closed by a putative double helix of 3 bp; however, the first 2 bp were not present or were too unstable to be observed. The third G-C base pair from the bottom is separated from the main double helix by a single adenine residue at position −2 (Fig. 5). As is often observed with single nucleotide purine bulges, the adenine residue does not extrude into solution, but intercalates into the double helix.

## DISCUSSION

The discovery of mutations located close to the splice-donor site of the intron after exon 10 of the tau gene has shown that overproduction of four-repeat tau isoforms is sufficient to produce a dementing disease (4, 5). To understand the mechanisms by which these mutations lead to increased splicing in of exon 10, we have investigated thermodynamic stability and three-dimensional structure of the tau exon 10 splicing regulatory element RNA and several mutant sequences. The NMR data establish that the 25 nt-long sequence forms a stem loop, as proposed (4, 5). The stem consists of a single stable G-C base pair that is separated from a double helix of 6 bp by an unpaired adenine. The apical loop consists of 6 nt that adopt multiple conformations in rapid exchange. The structure differs from two proposed representations of the stem loop. One study showed a stem consisting of only the upper part (4), whereas another study proposed a lower stem with 3 bp, a bulged adenine and an upper stem of 7 bp, with a 4-nt loop (5). The 2 bp in the lower part of the stem were probably too unstable to be observed, whereas the proposed G·U base pair at the boundary between the stem and the loop is not present. The unpaired adenine at position −2 is intercalated within the double-helical region. If the thermodynamic stability of the stem loop is critical for regulation, this structural feature could play an important role in modulating splice site utilization by limiting the overall thermodynamic stability of the stem loop. It is possible that the lower part of the stem encompasses an additional 5 nt not included in the structure studied here, adding a bulged C and two G-C base pairs. To date, no mutations have been found in the lower stem.

Known FTDP-17 mutations are located in the upper part of the stem, where they destabilize the stem-loop structure and reduce its thermodynamic stability. The largest drop in temperature was observed for the +3 mutation, and the NMR data show that the structure of the stem loop is severely affected by this mutation. The stem-loop structure is preserved for each of the other FTDP-17 mutations, but the thermodynamic stability is reduced in each case. The +14 and −1 mutations produced a large reduction in melting temperature, whereas the effects of the +13 and +16 mutations were smaller. Mutations that restore base pairing of the +3 and +13 mutations increased thermodynamic stability. Thus, the compensatory change for the +3 mutation increased the melting temperature from 51°C to 64°C, the same temperature as that of the regulatory element with the +13 mutation. The difference with the melting temperature of the wild-type sequence probably is explained by an A-U base pair instead of the wild-type G-C, which is insufficient to restore a melting temperature of 70°C. The introduction of a C-G base pair instead of the wild-type U-A to compensate for the +13 mutation gave a melting temperature of approximately 80°C.

The reductions in stem-loop stability resulting from the FTDP-17 mutations correlate with the results from exon trapping experiments. The +3 mutation produced the largest increase in the splicing in of exon 10, followed by the +14 mutation. The effects of the +13 and +16 mutations were smaller. The effects of the +3 mutation on the splicing in of exon 10 were similar to those of the S305N mutation at position −1 (24), which also is expected to lead to increased binding of U1 snRNA. However, the +3 mutation led to a larger reduction in melting temperature of the stem loop than the mutation at position −1.

The present findings provide strong support for the proposal that an intact stem-loop structure is necessary to ensure a correct ratio of three-repeat to four-repeat tau isoforms in adult human brain. They lead to the prediction that species that express six tau isoforms have a stable stem-loop structure at the boundary between exon 10 and the intron after exon 10. The same may not be true of species, such as rodents, that express only four-repeat tau in adult brain (29, 30). Mechanistically, access of the mRNA splicing machinery to the exon-intron junction simply could be regulated by the thermodynamic stability of the stem loop. A stable stem-loop

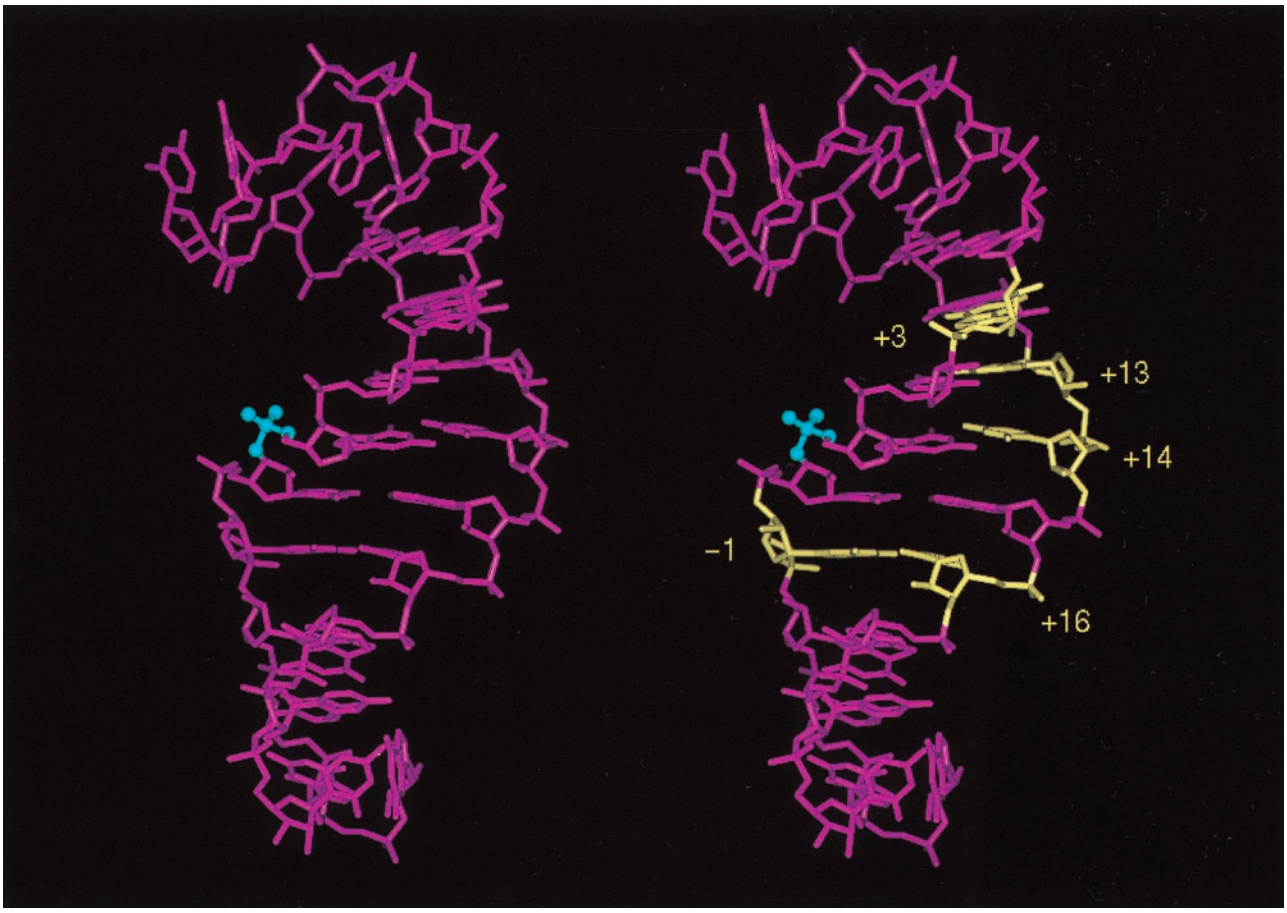


FIG. 4. Three-dimensional structure of human tau exon 10 splicing regulatory element. Two identical structures are shown, with the phosphate at the exon-intron junction identified in blue. Known FTDP-17 mutations in the stem-loop structure are highlighted in yellow on the right. They include the intronic mutations at positions +3, +13, +14, and +16, as well as the S305N mutation at position −1.

structure would reduce access, but mutations in the stem loop would unmask the splice junction, leading to increased production of exon 10-containing transcripts. Alternatively, or in addition, a stem loop of defined sequence and structure could be required for specific recognition by a trans-acting protein factor. As observed in other systems (31, 32), such a protein could recognize the identity of unpaired nucleotides in the context of a correctly folded stem-loop structure. A disrupted or less stable stem-loop structure would reduce protein binding, thereby increasing splice-site utilization. It remains to be determined whether the FTDP-17 mutations lead to increased splicing in of exon 10 through their effects on thermodynamic

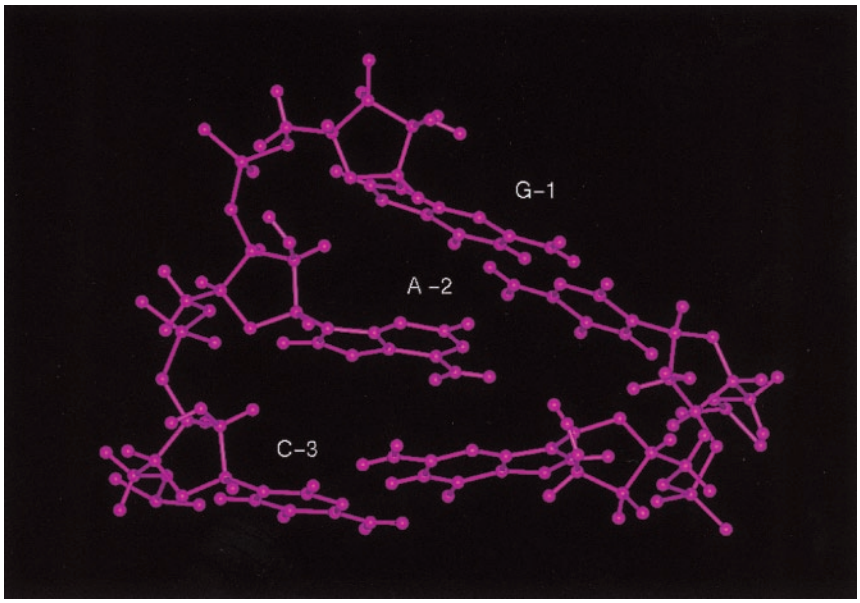


FIG. 5. Closeup view of the unpaired adenosine at position −2 intercalated between consecutive G-C base pairs.

stability of the stem-loop structure, through binding of a trans-acting protein factor, or through both mechanisms.

Increased levels of transcripts encoding four-repeat tau have been found by reverse transcription–PCR in brain tissue from FTDP-17 patients with the +14 and +16 mutations (4), and we have obtained similar results for the +3 mutation (data not shown). At the protein level, the net effect of the intronic mutations is a 1.5- to 2.5-fold increase in the ratio of four-repeat to three-repeat tau isoforms (5, 11, 15). This increase leads in turn to the assembly of four-repeat tau into the wide twisted ribbons characteristic of cases of FTDP-17 with intronic mutations (11, 33), possibly as a result of the excess four-repeat tau being unable to interact with microtubules (5, 25). Filament formation may be the gain of toxic function that is the "efficient" cause (in the Aristotelian sense) of FTDP-17.

We thank Mr. P. Cole for sample preparation, Dr. A. Ramos for advice on structure calculation, and Professor I. Tinoco, Jr. for advice on RNA thermodynamics and UV melting experiments. L.V. was supported by a studentship from the European Union; M.H. was supported by a postdoctoral fellowship from Innogenetics.

1. Spillantini, M. G. & Goedert, M. (1998) *Trends Neurosci.* **21,** 428–433.
2. Kertesz, A. & Munoz, D. (1998) *Arch. Neurol.* **55,** 302–304.
3. Poorkaj, P., Bird, T. D., Wijsman, E., Nemens, E., Garruto, R. M., Anderson, L., Andreadis, A., Wiederholt, W. C., Raskind, M. & Schellenberg, G. D. (1998) *Ann. Neurol.* **43,** 815–825.
4. Hutton, M., Lendon, C. L., Rizzu, P., Baker, M., Froelich, S., Houlden, H., Pickering-Brown, S., Chakraverty, S., Isaacs, A., Grover, A., *et al*. (1998) *Nature (London)* **393,** 702–705.
5. Spillantini, M. G., Murrell, J. R., Goedert, M., Farlow, M. R., Klug, A. & Ghetti, B. (1998) *Proc. Natl. Acad. Sci. USA* **95,** 7737–7741.
6. Dumanchin, C., Camuzat, A., Campion, D., Verpillat, P., Hannequin, D., Dubois, B., Saugier-Veber, P., Martin, C., Penet, C., Charbonnier, F., *et al*. (1998) *Hum. Mol. Genet.* **7,** 1825–1829.
7. Clark, L. N., Poorkaj, P., Wszolek, Z., Geschwind, D. H., Nasreddine, Z. S., Miller, B., Li, D., Payami, H., Awert, F., Markopoulou, K., *et al*. (1998) *Proc. Natl. Acad. Sci. USA* **95,** 13103–13107.
8. Rizzu, P., van Swieten, J. C., Joosse, M., Hasegawa, M., Stevens, M., Tibben, A., Niermeijer, M. F., Hillebrand, M., Ravid, R., Oostra, B. A., *et al*. (1999) *Am. J. Hum. Genet.* **64,** 414–421.
9. Iijima, M., Tabira, T., Poorkaj, P., Schellenberg, G. D., Trojanowski, J. Q., Lee, V. M.-Y., Schmidt, M. L., Takahashi, K., Nabika, K., Matsumoto, T., *et al*. (1999) *NeuroReport* **10,** 497–501.
10. Morris, H. R., Perez-Tur, J., Janssen, J. C., Brown, J., Lees, A. J., Wood, N. W., Hardy, J., Hutton, M. & Rossor, M. N. (1999) *Ann. Neurol.* **45,** 270–271.
11. Goedert, M., Spillantini, M. G., Crowther, R. A., Chen, S. G., Parchi, P., Tabaton, M., Lanska, D. J., Markesbery, W. R., Wilhelmsen, K. C., Dickson, D. W., *et al*. (1999) *Nat. Med.* **5,** 454–457.
12. Mirra, S. S., Murrell, J. R., Gearing, M., Spillantini, M. G., Goedert, M., Crowther, R. A., Levey, A. I., Jones, R., Green, J., Shoffner, J. M., *et al*. (1999) *J. Neuropathol. Exp. Neurol.* **58,** 335–345.
13. Bugiani, O., Murrell, J. R., Giaccone, G., Hasegawa, M., Ghigo, G., Tabaton, M., Morbin, M., Primavera, A., Carella, F., Solaro, C., *et al*. (1999) *J. Neuropathol. Exp. Neurol.* **58,** 595–605.
14. Hasegawa, M., Smith, M. J. & Goedert, M. (1998) *FEBS Lett.* **437,** 207–210.
15. Hong, M., Zhukareva, V., Vogelsberg-Ragaglia, V., Wszolek, Z., Reed, L., Miller, B. I., Geschwind, D. H., Bird, T. D., McKeel, D., Goate, A., *et al*. (1998) *Science* **282,** 1914–1917.
16. Dayanandan, R., van Slegtenhorst, M., Mack, T. G. A., Ko, L., Yen, S.-H., Leroy, K., Brion, J. P., Anderton, B. H., Hutton, M. & Lovestone, S. (1999) *FEBS Lett.* **446,** 228–232.
17. Goedert, M., Spillantini, M. G., Potier, M. C., Ulrich, J. & Crowther, R. A. (1989) *EMBO J.* **8,** 393–399.
18. Goedert, M., Spillantini, M. G., Jakes, R., Rutherford, D. & Crowther, R. A. (1989) *Neuron* **3,** 519–526.
19. Andreadis, A., Brown, M. W. & Kosik, K. S. (1992) *Biochemistry* **31,** 10626–10631.
20. Gustke, N., Trinczek, B., Biernat, J., Mandelkow, E. M. & Mandelkow, E. (1994) *Biochemistry* **33,** 9511–9522.
21. Goode, B. L. & Feinstein, S. C. (1994) *J. Cell Biol.* **124,** 769–782.
22. Goedert, M. & Jakes, R. (1990) *EMBO J.* **9,** 4225–4230.
23. Goedert, M., Spillantini, M. G., Cairns, N. J. & Crowther, R. A. (1992) *Neuron* **8,** 159–168.
24. Hasegawa, M., Smith, M. J., Iijima, M., Tabira, T. & Goedert, M. (1999) *FEBS Lett.* **443,** 93–96.
25. Goedert, M., Crowther, R. A. & Spillantini, M. G. (1998) *Neuron* **21,** 955–958.
26. Price, S. R., Oubridge, C., Varani, G. & Nagai, K. (1998) in *RNA-Protein Interactions: A Practical Approach,* ed. Smith, C. (Oxford Univ. Press, Oxford), pp. 37–74.
27. Lapham, J., Rife, J. P., Moore, P. B. & Crothers, D. M. (1997) *J. Biomol. NMR* **10,** 255–262.
28. Varani, G., Abou-ela, F. & Allain, F. H.-T. (1996) *Prog. NMR Spectr.* **29,** 51–127.
29. Goedert, M., Jakes, R., Crowther, R. A., Cohen, P., Vanmechelen, E., Vandermeeren, M. & Cras, P. (1994) *Biochem. J.* **301,** 871–877.
30. Götz, J., Probst, A., Spillantini, M. G., Schäfer, T., Jakes, R., Bürki, K. & Goedert, M. (1995) *EMBO J.* **14,** 1304–1313.
31. Klausner, R. D. & Harford, J. B. (1989) *Science* **246,** 870–872.
32. Valegard, K., Murray, J. B., Stockley, P. G., Stonehouse, N. J. & Liljas, L. (1994) *Nature (London)* **371,** 623–626.
33. Spillantini, M. G., Goedert, M., Crowther, R. A., Murrell, J. T., Farlow, M. J. & Ghetti, B. (1997) *Proc. Natl. Acad. Sci. USA* **94,** 4113–4118.